18èmes Journées Internationales de Thermique (JITH 2017)
Monastir (Tunisie), 25 - 27 Octobre 2017

Mathematical modeling and numerical simulation of a co-current humidifier used in desalination process

Hana Gouider [1], Leila Zili-Ghedira [2],Sassi Ben Nasrallah[3]

Université de Monastir - Ecole Nationale d'Ingénieurs de Monastir

5000 MONASTIR - TUNISIE

[1] E-mail: gouiderhana@hotmail.fr

[2]E-mail: leilazilighedra@yahoo.fr

[3]E-mail: sassi.bennasrallah@enim.rnu.tn

Abstract

The solar desalination systems with humidification-dehumidification are generally composed of an evaporator, a condenser and two solar collector's air and water.

We will study in this article a humidifier compounding from a porous medium. The mathematical model of heat and mass transfer used is deduced from Whitaker's theory.

The models usually used in the literature for this component can be deduced from the present model using simplifying assumptions.

Generally, the evaporators used are countercurrent whereas in this paper co-current evaporators will be used for practical and technical reasons. This model predicts temperature and humidity changes in the evaporator. A numerical study is conducted to the variables mentioned. These variables were obtained for wide ranges of air and water mass flow rates as well as for several water inlet temperatures.

Keywords: Desalination; Porous media; Humidification-Dehumidification; Co-current humidifier; mathematical model; numerical study

Nomenclature

$A_{\beta\sigma}$: area of the β-σ interface

Cp: specific heat $Jkg^{-1}K^{-1}$

D: diffusion coefficient m^2s^{-1}

G: gas mass flow rate $kgm^{-2}s^{-1}$

h_β: enthalpy of the β-phase Jkg^{-1}

H: heat transfer coefficient $Wm^{-2}K^{-1}$

H_m: mass transfer coefficient kg $m^{-2}s^{-1}$

L: liquid mass flow rate $kgm^{-2}s^{-1}$

L_v: evaporation latent heat Jkg^{-1}

$\dot{m}$: mass rate of evaporation $kgm^{-3}s^{-1}$

$n_{\beta\sigma}$=- $n_{\sigma\beta}$ outwardly directed unit normal vector pointing from β-phase toward theσ-phase

S: surface area per unit volume of the porous media m^2m^{-3}

t: time s

T: temperature K

v_β:velocity of the β-phase ms^{-1}

V: averaging volume m^3

V_β : volume of the β-phase contained within the averaging volume, m^3

w_{lg} : speed of displacement of the liquid–vapor interface, ms^{-1}

x : distance m

Greek symbols

α: coefficient; α = 1 for humidifier and α = -1 for condenser

ρ_β: density in the β-phase $kg.m^{-3}$

λ_β: thermal conductivity of the β-phase $Wm^{-1}K^{-1}$

ω: absolute humidity $kg.kg^{-1}$

ε_β: volume fraction of the β-phase

Subscripts

a	dry air
efβ	effective value of the β phase
g	gas
l	liquid
s	solid
sat	saturation

v vapor

1. Introduction

During the past three decades, numerous desalination methods have been proposed due to the increasing demand for fresh (drinking) water. Currently, reverse osmosis (RO) and multi-stage flash (MSF) are the most used. In addition, mechanical vapor compression (MVC) and multiple effect evaporation (MED) are used on limited scales to produce water from the sea [1, 2]. These technologies are expensive for small amounts of fresh water and cannot be used in locations such as islands or remote areas where maintenance facilities and energy supply are limited [3].

Desalination with Humidification-Dehumidification process (HDD) is the efficient and promising means of small and medium fresh water production so theses systems are the subject of numerous researchs [4-10] targeting the enrichment of the plant performance.

To develop heat and mass transfers, some authors [7,11-13] exploited packing structure in humidifier and fin-tube condenser type. Thus the humidifier is instituted by three phases (solid, liquid (water) and air).The mathematical modeling of heat transfer and mass in the humidifier is difficult to achieve because the complicated distribution of three phases. The common publications treat the humidifier use mass and energy balance of most HDD installation for determining the temperature and humidity inlet and outlet of components [14-19]. They frequently use empirical correlations for heat and mass coefficients. Most mathematical modeling of heat and mass transfers are presented without justification and without determination of their validity conditions.

The study of co-current humidifier is not frequent in the literature although it is used in certain systems for practical reasons. The aim of this paper is the improvement of a laborious mathematical model with explanations and the determination of the validity conditions of the usually used model in HDD process. The co-current humidifier is considered as porous media constituted by three phases (liquid, solid, gas). A mathematical model valuable at the pore scale is presented, and then a scale changing is mentioned to develop this mathematical model valuable at a macroscopic scale.

The numerical tool developed is successfully validated using experimental results from literature. The two abovementioned models are compared and conclusions are drawn back. The thermo-physical properties of this humidifier and packing materials (heat capacity and conductivity were examined.

2. Mathematical modeling

This concurrent humidifier is considered as porous medium constituted by a solid, water and air. The gas is identified as the g-phase, the solid as the s-phase and the liquid as the l-phase. In this paper, the two phase velocity fields are known.

2.1. Pore-scale formulations

By using mechanical and thermodynamic laws [20], the heat and mass transfer formulas are developed in each phase. We pass from a microscopic view where the size of the representative volume is small with regard to the pores, to a macroscopic view where the size of the representative volume is large with regard to the pores.

Continuity equations for the gaseous phase:

In the gaseous phase:

$$\frac{\partial \rho_g}{\partial t} + \nabla.(\rho_g v_g) = 0 \tag{1}$$

$$\frac{\partial \rho_v}{\partial t} + \nabla.(\rho_v v_v) = 0 \tag{2}$$

$$\rho_v v_v = \rho_v v_g - \rho_g D_v \nabla(\rho_v/\rho_g) \tag{3}$$

$$\rho_g = \rho_v + \rho_a \tag{4}$$

Mass balance equations for the gaseous phase:

$$v_g = 0, \text{ at the g-s interface} \tag{5}$$

$$n_{lg}.\rho_g(v_g - w_{lg}) = n_{lg}.\rho_l(v_l - w_{lg}) \text{ at the l-g interface} \tag{6}$$

$$v_v = 0, \text{ at the g-s interface} \tag{7}$$

$$n_{lg}.\rho_v(v_v - w_{lg}) = n_{lg}.\rho_l(v_l - w_{lg}) \text{ at the l-g interface} \tag{8}$$

Here w_{lg} is the liquid–gas interface velocity and n_{lg} represents the unit normal directed from the l-phase towards the g-phase. ρ_g, ρ_l and ρ_v, are gaseous, liquid and vapor densities, D_v is the vapor diffusivity in the gaseous phase, v_g is the gaseous velocity:

$$v_g = \frac{\rho_v v_v + \rho_a v_a}{\rho_g} \tag{9}$$

Continuity equation for the liquid phase:

In the liquid phase:

$$\frac{\partial \rho_l}{\partial t} + \nabla.(\rho_l v_l) = 0 \text{, in the l-phase} \tag{10}$$

$$v_l = 0, \text{ at the l-s interface} \tag{11}$$

Energy equations:

Solid phase:

$$\frac{\partial(\rho_s h_s)}{\partial t} = \nabla.(\lambda_s \nabla T_s) \tag{12}$$

Liquid phase:

$$\frac{\partial(\rho_l h_l)}{\partial t} + \nabla.(\rho_l h_l v_l) = \nabla.(\lambda_l \nabla T_l) \tag{13}$$

Gaseous phase:

This represents dry air and vapor

$$\frac{\partial(\rho_g h_g)}{\partial t} + \nabla.(\rho_g h_g v_g) = \nabla.(\lambda_g \nabla T_g) \tag{14}$$

h_β is the enthalpy of the β-phase (β = l, g, s). λ_g, λ_l and λ_s are the gaseous, liquid and solid thermal conductivities. Here we have neglected compression work, viscous dissipation and radiation exchange.

Heat balance equations:

The boundary conditions at the liquid–solid and vapor–solid interfaces express continuity of both temperatures and heat fluxes.

$T_g = T_s$, $n_{gs}.(\lambda_g \nabla T_g) = n_{gs}.(\lambda_s \nabla T_s)$ at the g-s interface (15)

$T_l = T_s$, $n_{ls}.(\lambda_l \nabla T_l) = n_{ls}.(\lambda_s \nabla T_s)$ at the l-s interface (16)

The boundary conditions at the liquid–vapor interface are written as:

$T_g = T_l = T^{sat}$, at the l-g interface (17)

$n_{lg}.(-\lambda_g \nabla T_g + \rho_g h_g (v_g - w_{lg})) = n_{lg}.(-\lambda_l \nabla T_l + \rho_l h_l (v_l - w_{lg}))$, at the l-g interface (18)

2.2. Volume averaging

We define an averaging volume V at each point of the packing. V must be large compared with the pore scales characteristics length l_l, l_g and l_s. Two different averages are observed: the phase average $\langle \Psi_\beta \rangle$ and the intrinsic β-phase average $\langle \Psi_\beta \rangle^\beta$:

$$\langle \Psi_\beta \rangle = \frac{1}{V} \int_{V_\beta} \Psi_\beta dV, \qquad \langle \Psi_\beta \rangle^\beta = \frac{1}{V_\beta} \int_{V_\beta} \Psi_\beta dV, \qquad \langle \Psi_\beta \rangle = \varepsilon_\beta \langle \Psi_\beta \rangle^\beta \tag{19}$$

V_β represents the volume of the β-phase contained within V and ε_β is the volume fraction of the β-phase. The averages of the spatial and temporal derivation are obtained using the general transport theorem and the spatial averaging theorem Whitaker [21]:

$$\langle \nabla \Psi_\beta \rangle = \nabla \langle \Psi_\beta \rangle + \sum_{\alpha \neq \beta} \frac{1}{V} \int_{A_{\beta\alpha}} \Psi_\beta n_{\beta\alpha} dA \tag{20}$$

$n_{\beta\alpha}$ represents the unit normal directed from the β- phase towards the α-phase and $A_{\beta\alpha}$ is the β–α interface.

$$\left\langle \frac{\partial \Psi_\beta}{\partial t} \right\rangle = \frac{\partial \langle \Psi_\beta \rangle}{\partial t} - \sum_{\alpha \neq \beta} \frac{1}{V} \int_{A_{\beta\alpha}} \Psi_\beta w_{\beta\alpha} n_{\beta\alpha} dA \tag{21}$$

A modified spatial averaging theorem gives (Gray 1975) [22]

$$\left\langle \nabla \Psi_\beta \right\rangle = \varepsilon_\beta \nabla \left\langle \Psi_\beta \right\rangle^\beta + \sum_{\alpha \neq \beta} \frac{1}{V} \int_{A_{\beta\alpha}} \tilde{\Psi}_\beta n_{\beta\alpha} dA \tag{22}$$

The point values Ψ_β in the β-phase are related to the intrinsic average $\left\langle \Psi_\beta \right\rangle^\beta$ and the pore-scale deviation $\tilde{\Psi}_\beta$ according to Gray's [22] spatial decomposition:

$$\tilde{\Psi}_\beta = \Psi_\beta - \left\langle \Psi_\beta \right\rangle^\beta \tag{23}$$

2.2.1. Mass conservation equations

$$\dot{m} = \frac{1}{V} \int_{A_{gl}} \rho_l \left(v_l - w_{lg} \right) n_{gl} dA = -\frac{1}{V} \int_{A_{gl}} \rho_g \left(v_g - w_{lg} \right) n_{gl} dA \tag{24}$$

The volume averaging of the pore-scale mass transport equations (10), (1) and (2) leads to:

$$\frac{\partial \varepsilon_l \rho_l}{\partial t} + \nabla . \left(\rho_l \left\langle v_l \right\rangle \right) = -\dot{m} \tag{25}$$

$$\frac{\partial \varepsilon_g \left\langle \rho_g \right\rangle^g}{\partial t} + \nabla . \left\langle \rho_g v_g \right\rangle = \dot{m} \tag{26}$$

$$\frac{\partial \varepsilon_g \left\langle \rho_v \right\rangle^g}{\partial t} + \nabla . \left\langle \rho_v v_g \right\rangle = \nabla . \left\{ \left\langle \rho_g D \nabla \left(\frac{\rho_v}{\rho_g} \right) \right\rangle \right\} + \dot{m} \tag{27}$$

We assume that the mass transfer at the interface can be modeled using a mass transfer coefficient Hm (ASHRAE Handbook of Fundamentals, 1997):

$$\dot{m} = H_m S \left(\omega^{sat} - \omega \right) \tag{28}$$

2.2.2. Energy conservation equations

$$\begin{aligned} & C_{pg} \left\langle \rho_g \right\rangle \frac{\partial \left\langle T_g \right\rangle^g}{\partial t} + C_{pg} \left\langle \rho_g \right\rangle^g \left\langle v_g \right\rangle \nabla \left\langle T_g \right\rangle^g - \dot{m} C_{pg} \left(T^{sat} - \left\langle T_g \right\rangle^g \right) \\ & = \nabla . \left(\lambda_{efg} \nabla \left\langle T_g \right\rangle^g \right) + \alpha H_{gl} S_{gl} \left(T^{sat} - \left\langle T_g \right\rangle^g \right) + H_{gs} S_{gs} \left(\left\langle T_s \right\rangle^s - \left\langle T_g \right\rangle^g \right) \end{aligned} \tag{29}$$

$$\begin{aligned} & \varepsilon_l \rho_l C_{pl} \frac{\partial \left\langle T_l \right\rangle^l}{\partial t} + \rho_l C_{pl} \left\langle v_l \right\rangle \nabla \left\langle T_l \right\rangle^l + \dot{m} C_{pl} \left(T^{sat} - \left\langle T_l \right\rangle^l \right) \\ & = \nabla . \left[\lambda_{efl} \nabla \left\langle T_l \right\rangle^l \right] + \alpha H_{lg} S_{lg} \left(\left\langle T_l \right\rangle^l - T^{sat} \right) + H_{ls} S_{ls} \left(\left\langle T_s \right\rangle^s - \left\langle T_l \right\rangle^l \right) \end{aligned} \tag{30}$$

$$\begin{aligned} & \varepsilon_s \rho_s C_{ps} \frac{\partial \left\langle T_s \right\rangle^s}{\partial t} \\ & = \nabla . \left(\lambda_{efs} \nabla \left\langle T_s \right\rangle^s \right) + H_{sg} S \left(\left\langle T_g \right\rangle^g - \left\langle T_s \right\rangle^s \right) + H_{sl} S_{sl} \left(\left\langle T_l \right\rangle^l - \left\langle T_s \right\rangle^s \right) \end{aligned} \tag{31}$$

$$\frac{\partial \varepsilon_g \langle \rho_v \rangle^g}{\partial t} + \nabla\left(\langle \rho_v \rangle^g \langle v_g \rangle\right) = \nabla\left\{\langle \rho_g \rangle^g D_{geff} \nabla\left(\frac{\langle \rho_v \rangle}{\langle \rho_g \rangle}\right)\right\} + H_m S\left(\omega^{sat} - \omega\right) \tag{32}$$

To simplify the equations set, we use the following hypotheses:

Assumption 1:

We assume that there is a local thermal equilibrium between the liquid and the solid phases:

$$\langle T_s \rangle^s = \langle T_l \rangle^l \tag{33}$$

Eqs. (30) and (31) give:

$$\begin{aligned}&\left(\varepsilon_s \rho_s C_{ps} + \varepsilon_l \rho_l C_{pl}\right)\frac{\partial \langle T_l \rangle^l}{\partial t} + \rho_l C_{pl} \langle v_l \rangle \nabla \langle T_l \rangle^l + \dot{m} C_{pl}\left(T^{sat} - \langle T_l \rangle^l\right) \\ &= \nabla.\left[\left(\lambda_{efl} + \lambda_{efs}\right)\nabla \langle T_l \rangle^l\right] + H_{lg} S_{lg}\left(\langle T_l \rangle^l - T^{sat}\right) + H_{sg} S_{sg}\left(\langle T_g \rangle^g - \langle T_s \rangle^s\right)\end{aligned} \tag{34}$$

Assumption 2:

The liquid film wets completely the solid: Ssg=0.

Eqs.(29) and (34) become:

$$C_{pg} \langle \rho_g \rangle \frac{\partial \langle T_g \rangle^g}{\partial t} + C_{pg} \langle \rho_g \rangle^g \langle v_g \rangle \nabla \langle T_g \rangle^g - \dot{m} C_{pg}\left(T^{sat} - \langle T_g \rangle^g\right) = \nabla.\left(\lambda_{efg} \nabla \langle T_g \rangle^g\right) + H_{gl} S_{gl}\left(T^{sat} - \langle T_g \rangle^g\right) \tag{35}$$

$$\left(\varepsilon_s \rho_s C_{ps} + \varepsilon_l \rho_l C_{pl}\right)\frac{\partial \langle T_l \rangle^l}{\partial t} + \rho_l C_{pl} \langle v_l \rangle \nabla \langle T_l \rangle^l + \dot{m} C_{pl}\left(T^{sat} - \langle T_l \rangle^l\right) = \nabla.\left(\left(\lambda_{efl} + \lambda_{efs}\right)\nabla \langle T_l \rangle^l\right) + H_{lg} S_{lg}\left(\langle T_l \rangle^l - T^{sat}\right) \tag{36}$$

The heat of vaporization and the mass rate of evaporation are related to the saturation temperature by the following expression:

$$\dot{m} \Delta h = H_{lg} S_{lg}\left(\langle T_l \rangle^l - T^{sat}\right) - H_{gl} S_{gl}\left(T^{sat} - \langle T_g \rangle^g\right) \tag{37}$$

Finally we get the model usually used:

$$\frac{dT_l}{dz} = \frac{H_{lg} S\left(T_l - T^{sat}\right)}{L C_{pl}} \quad \text{for the l-phase} \tag{38}$$

$$\frac{dT_g}{dz} = \frac{\mathrm{H_{gl}} S\left(T^{sat} - T_g\right)}{G.C_{pg}} \quad \text{for the g-phase} \tag{39}$$

$$G\frac{d\omega}{dz} = H_m S\left(\omega^{sat} - \omega\right) \tag{40}$$

3. Numerical study

This numerical study is valid for both co-current and counter-current humidifier. The packing, illustrated in figure 1, contains multiple vertical plates. We have elaborated a numerical non-stationary two-dimensional general code accounting for conduction term. The governing equations of the first complete model are (32), (35) and (36).

A numerical comparison between the complete model elaborated and the simplified usually used model is carried out. The equations of the simplified model are the equations from (37) to (40).

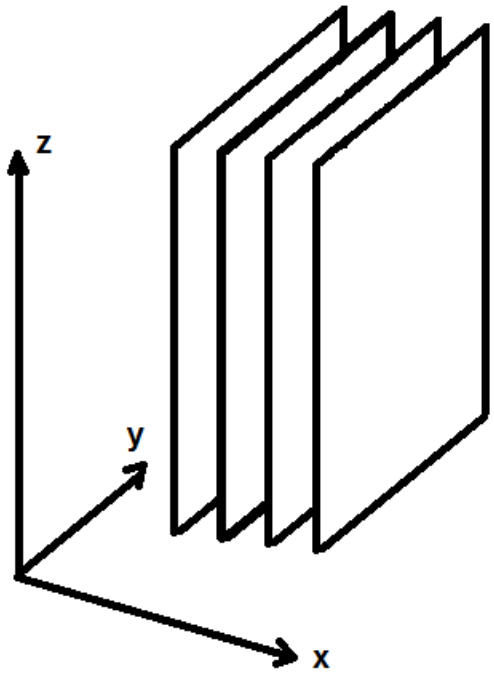

Figure 1: Schematic of the film-type packing with coordinates

3.1. Numerical resolution

In this case, we use the finite domain method because the system of differential equations obtained is not linear. This method consists of defining a grid of points and constructing a control domain around each node (see figure 2). This method guarantees the conservation of the flux and inhibits the generation of parasitic sources. An Upwind scheme is conciliated for discretization. The grid used and the time step are uniform.

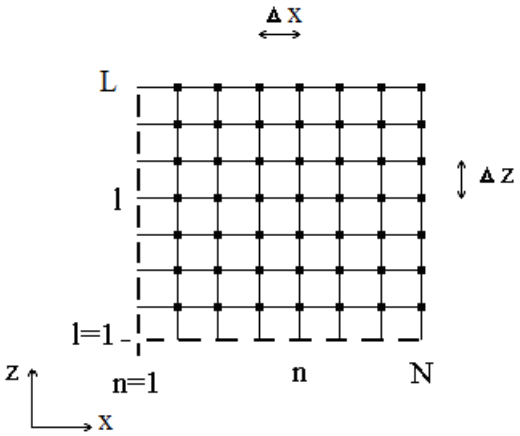

Figure 2: Numerical grid

The validation of this numerical code was done by comparison with the experimental results obtained in the article of Farhad Gharagheizi [24] which concern a counter-current cooling tower of packing of PVC (humidifier) with cross section area of 0.5x0.5 m^2 and 1.5 m height.

The numerical results and the experimental results of the article is shown in the following table; it noted that the maximum relative error is 2.16% (Tableau 1).

L (Kg/s)	G (Kg/s)	L/G	T experimental (°C)	T code (°C)	Relative error (%)
0.3	0.64	0.4722	32.77	33.08	**0.94**
0.3	0.52	0.5812	33.22	33.11	**0.33**
0.3	0.26	1.1625	33.77	33.27	**1.48**
0.25	0.64	0.3935	32.33	33.03	**2.16**
0.25	0.52	0.4844	32.77	33.07	**0.91**
0.25	0.4	0.6297	33.5	33.12	**1.13**
0.2	0.64	0.3148	32.22	32.96	**2.29**
0.2	0.52	0.3875	32.33	33	**2.07**
0.2	0.4	0.5037	32.94	33.06	**0.36**

Tableau 1:Comparison between numerical and experimental results of [24].

3.2. Results and interpretation

The packaging of the humidifier, in the literature, is made from different materials such as paper [20, 25], wood [26], PVC [24, 27], aluminum and copper [19]...

To make a comparison between the complete non-stationary model with the conduction term and the simplified stationary model without conduction term, a numerical simulation is made for a co-current

humidifier with a cross-section of 0.9 x 0.9 m² and 1, 4 m height and the packing is formed of 20 vertical plates.

The initial conditions: water and air temperatures are, respectively, 40°C and 25°C.

We test diver materials forming the humidifier plates ranging from low conductivity materials such as paper to high conductivity materials such as cooper (see Table 2). The results of this study are presented for copper as it has the most important conductivity.

We examinate the following cases:

- Water flow rate is L = 0.1 kg/s and water by air flow rate L/G takes the values 0.05-0.1-0.2-0.5-1, then air flow rate G is equal to 2-1-0.5-0.2-0.1kg/s.
- Air flow rate is G = 2 kg/s and water by air flow rate L/G takes the values 0.05-0.1-0.25-0.5-1, then water flow rate L is equal to 0.1-0.2-0.5-1-2kg/s.

Material	**Density** ρ_s **(kg/m^3)**	**Specific heat capacity** C_{ps} **(J/kg K)**	**Conductivity** λ_s **(W/m K)**
Paper	700	1200	0.12
Wood	500	2300	0.14
PVC	1190	1046	0.17
Aluminum	2700	797	237
Copper	8930	382	399

Table 2: Thermo-physical characteristics of humidifier packing materials.

From figure 3, we notice that for a fixed value of water flow rate, the water outlet temperature decreases with the increase of air flow rate and for a given air flow rate, this temperature drops with the drop of water flow rate (Figure 4). So, evaporation increases and water outlet temperature decreases with the decrease of L/G.

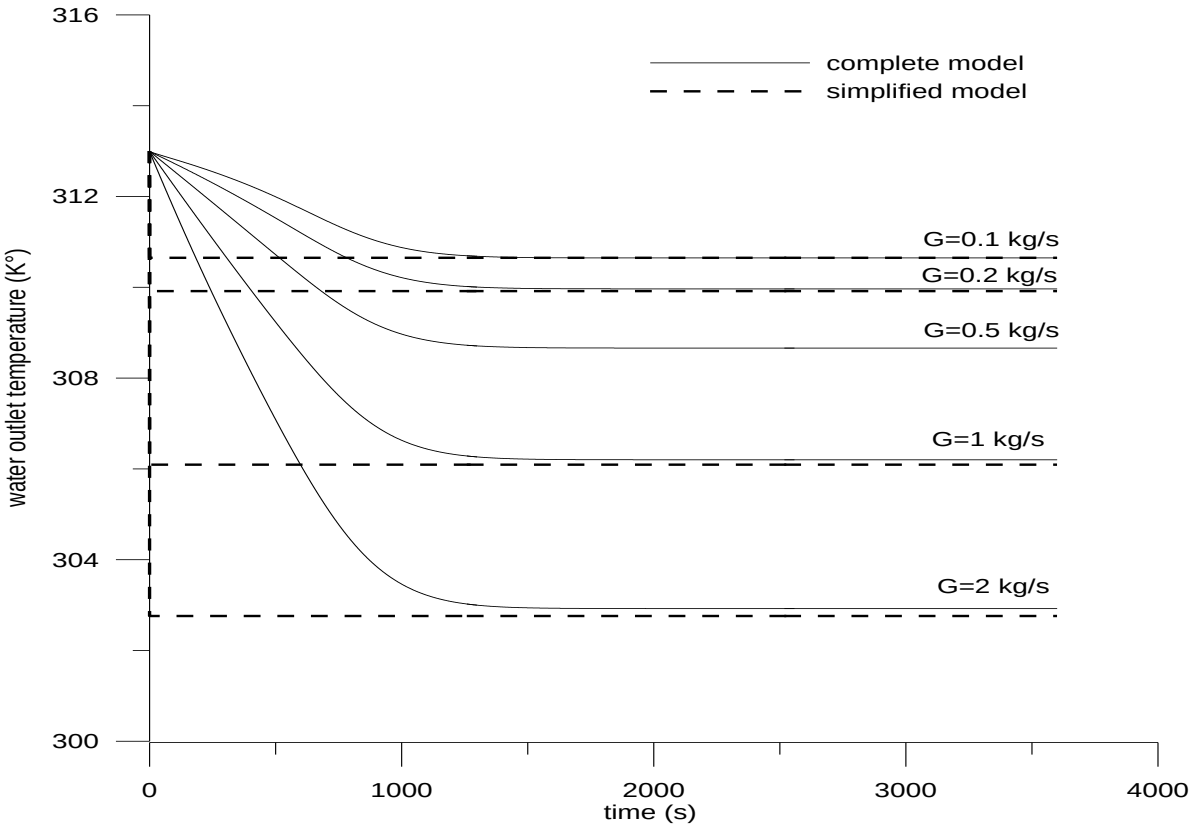

Figure 3 : Water outlet temperature for L = 0.1 kg/s and G ranging from 0.1 to 2 kg/s

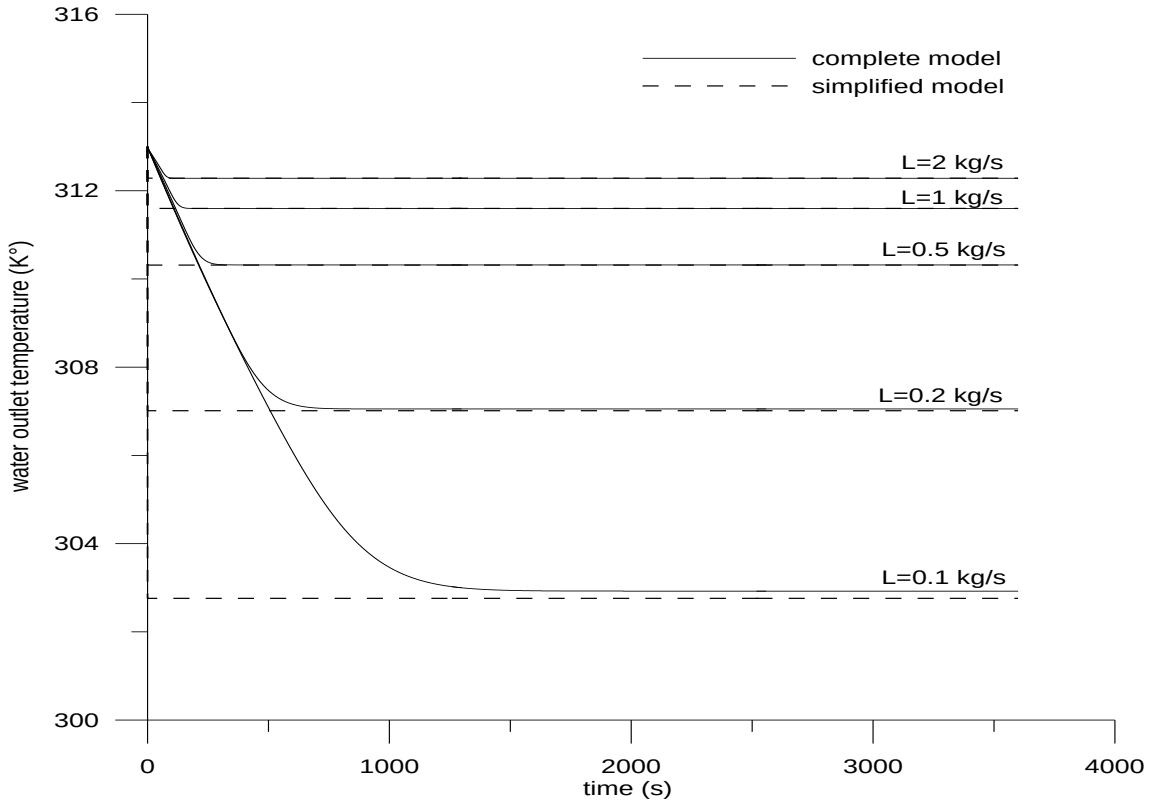

Figure 4: Water outlet temperature for G = 2kg/s and L ranging from 0.1 to 2 kg/s.

The outlet air temperature is lesser for higher air flow rate for a fixed water flow rate (Figure 5) and also for lower water flow rate for a fixed air flow rate (Figure 6). Then air outlet temperature diminishes with the diminution of L/G.

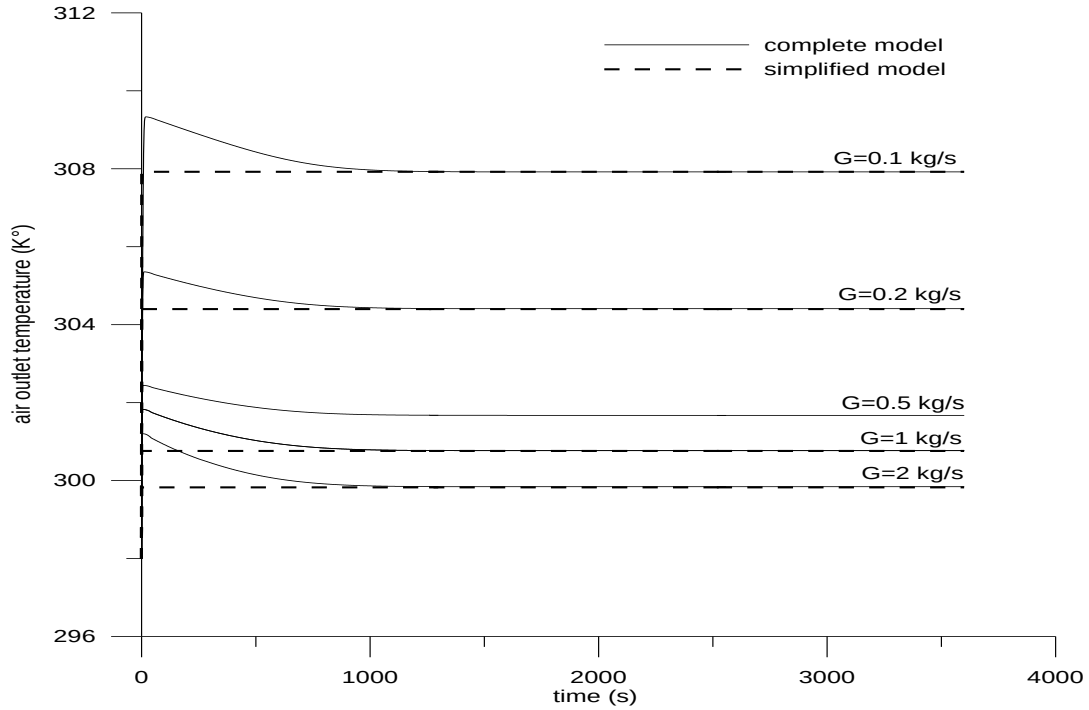

Figure 5: Air outlet temperature for L = 0.1 kg/s and G ranging from 0.1 to 2 kg/s

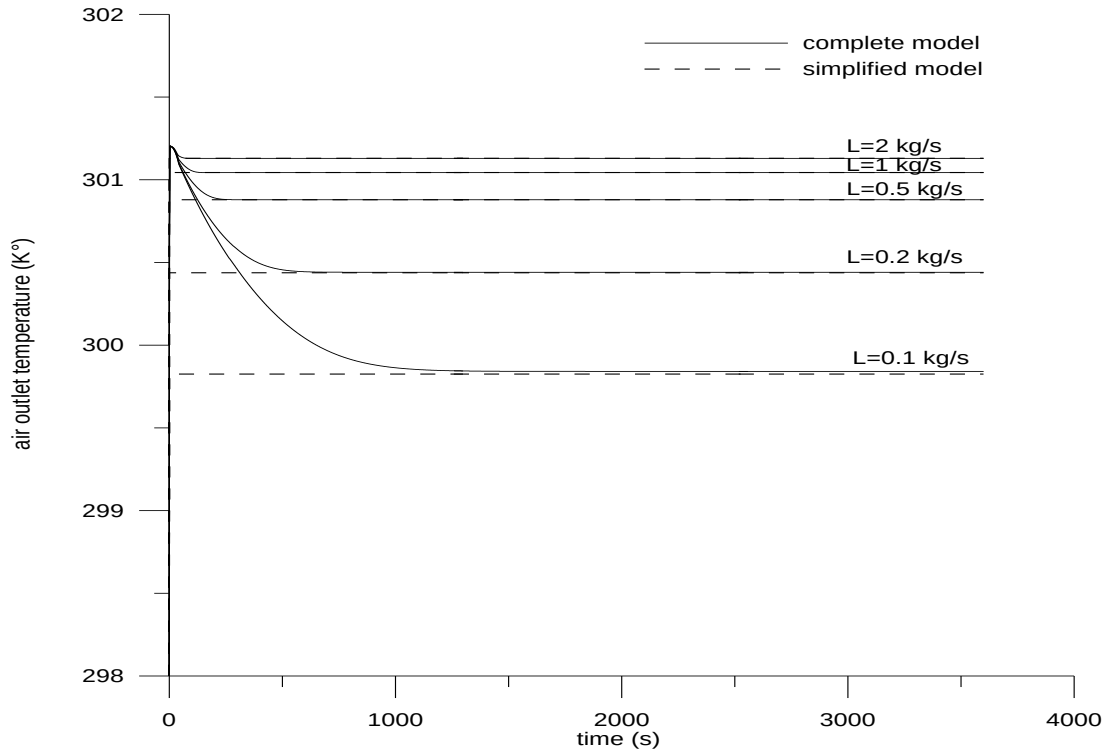

Figure 6: Air outlet temperature for G = 2kg/s and L ranging from 0.1 to 2 kg/s.

The evaporation is more important if the air flow rate is higher for a given water flow rate (Figure 7) and the water flow rate is lower for a given air flow rate (figure 8).

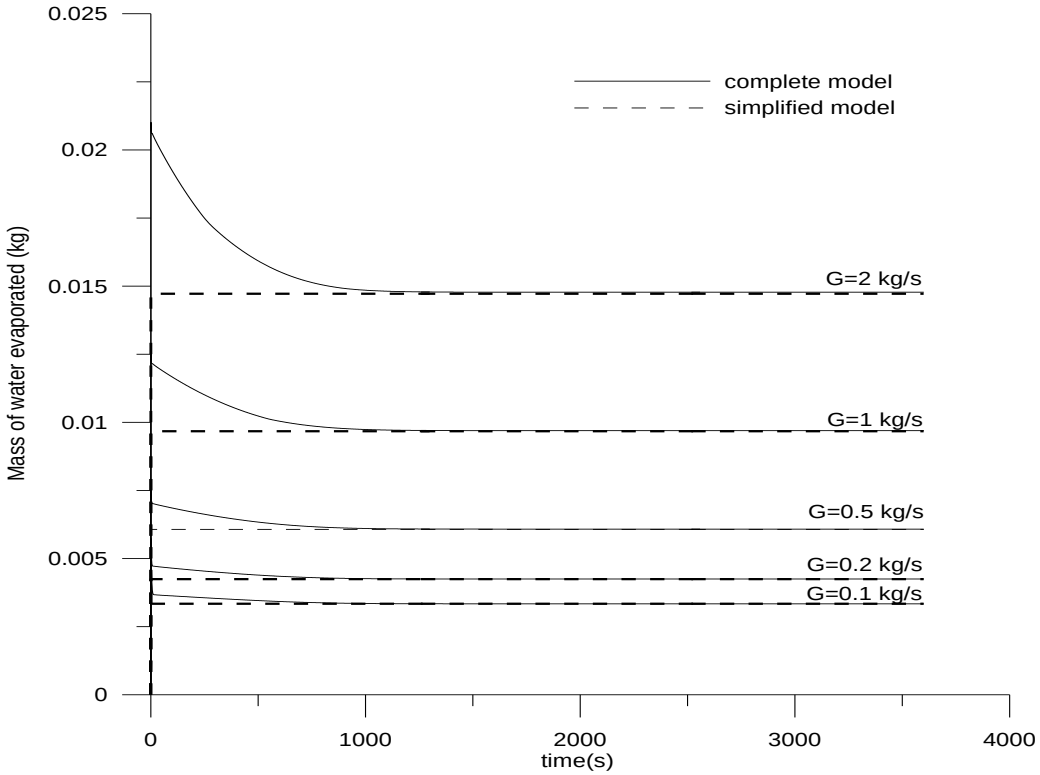

Figure 7: Mass of water evaporated for L = 0.1 kg/s and G ranging from 0.01 to 2 kg/s

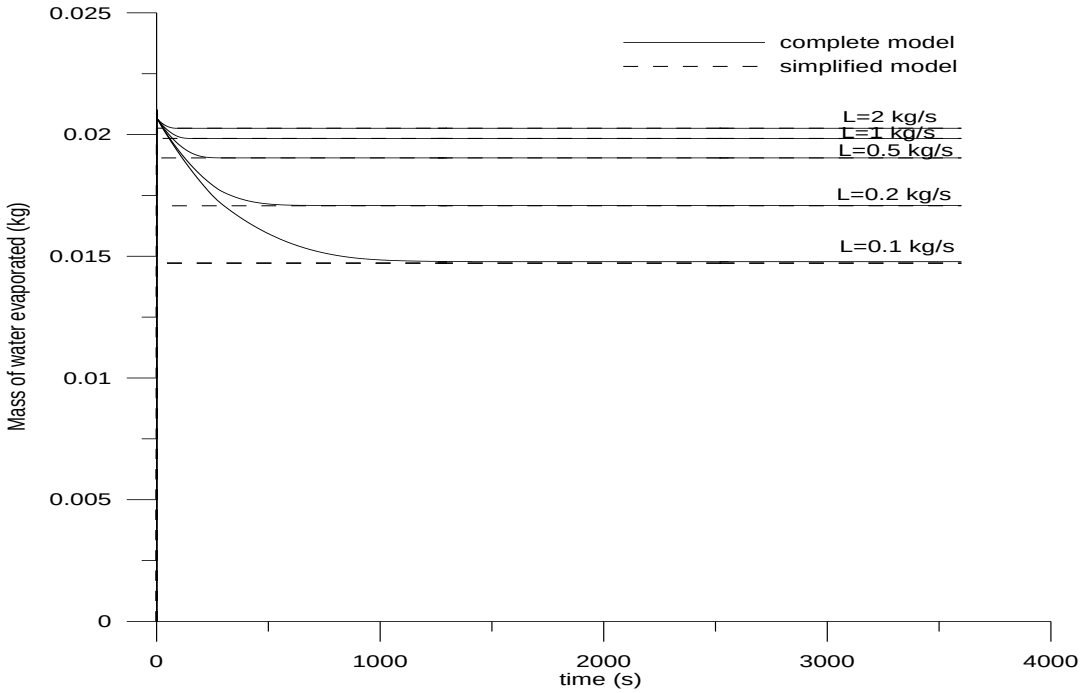

Figure 8: Mass of water evaporated for G = 2 kg/s and L ranging from 0.01 to 2 kg/s.

Thus, it's confirmed that humidifier yield is enhanced with L/G decrease.

When fixing the water flow rate, the difference between the two models is more important for L/G = 0.05 and it decreases with the increasing of L/G. This shows that the difference between the two models is more important when air flow rate is amplified, for a given water flow rate.

In the same case, we describe for a fixed air flow rate the difference between the two models is higher when the water flow rate is reduced, which means that when L/G is lower.

Which is explained by the negligence of the terms in the simple $\dot{m}C_{pl}\left(T^{sat}-T_l\right)$ and $\dot{m}C_{pg}\left(T^{sat}-T_g\right)$ comparatively with the complete model, and then when evaporation increases with the increase of L/G, the difference between the two models is more appreciable.

We use several materials packing which have different densities, specific heat capacities and conductivities. Their thermo-physical propertie of packing materials effects were examined.

For L = 0.1 kg/s and G = 2kg/s,(figure 9), we illustrate that water outlet temperature is a little bit lower when considering lower conductivity λ_s;

It is the lowest for paper and the highest for copper. For water and air outlet temperatures, the steady state is quickly reached for a lower calorific capacity $\rho_s C_{ps}$; It is rapid for paper than for copper (Figures 9, 10), but the difference is negligible. From Figure 11, the consideration of copper and aluminum as packaging material improves evaporation slightly rather than considering PVC, wood or paper, but this difference remains low.

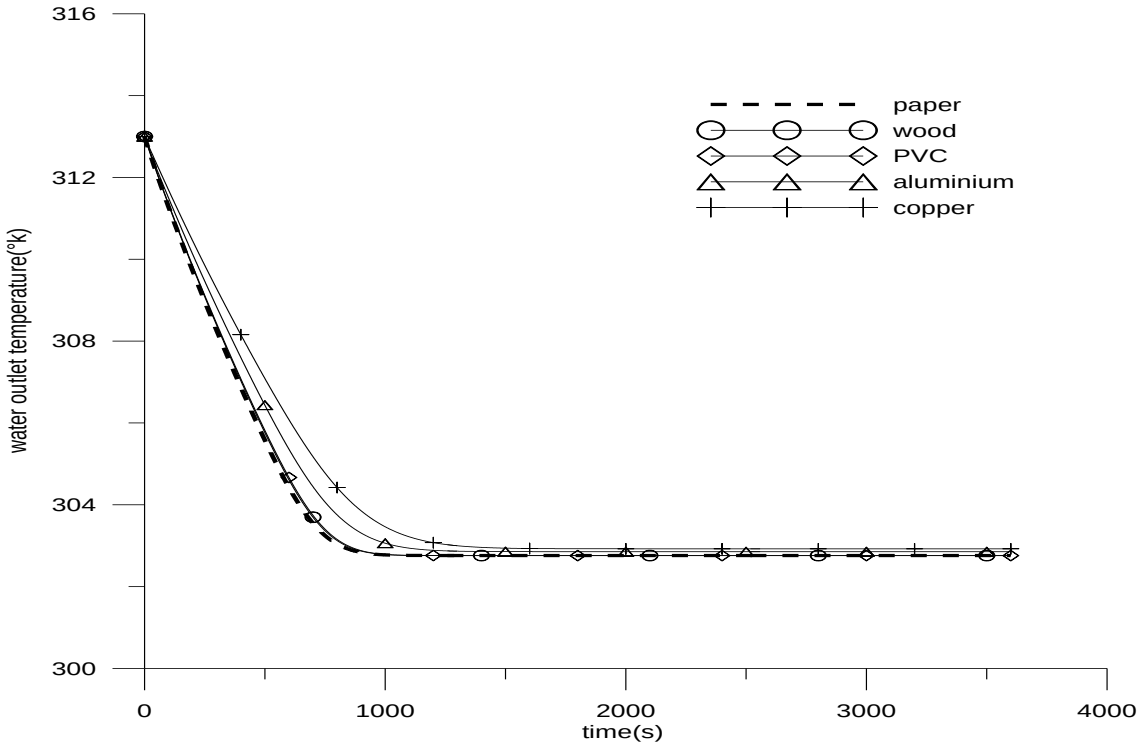

Figure 9: Water outlet temperature for different packing materials at L = 0.1 kg/s and G = 2 kg/s.

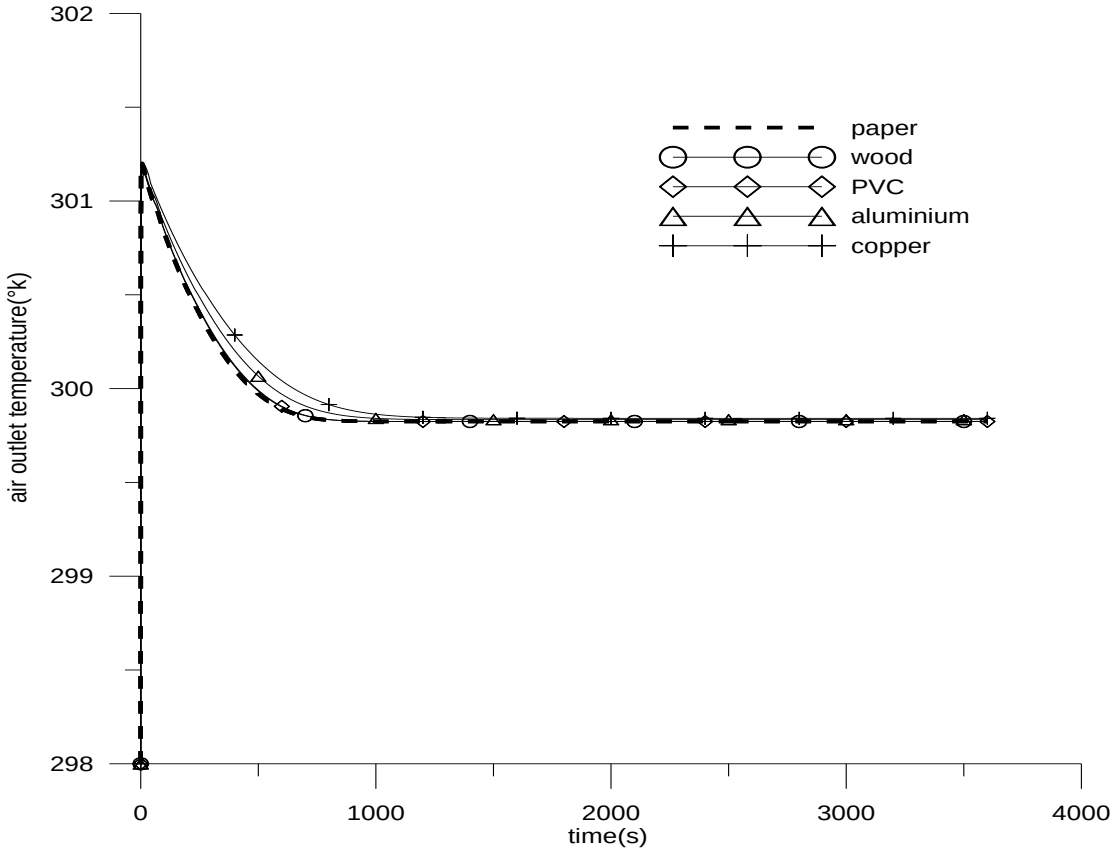

Figure 10: Air outlet temperature for different packing materials at L = 0.1 kg/s and G = 2 kg/s.

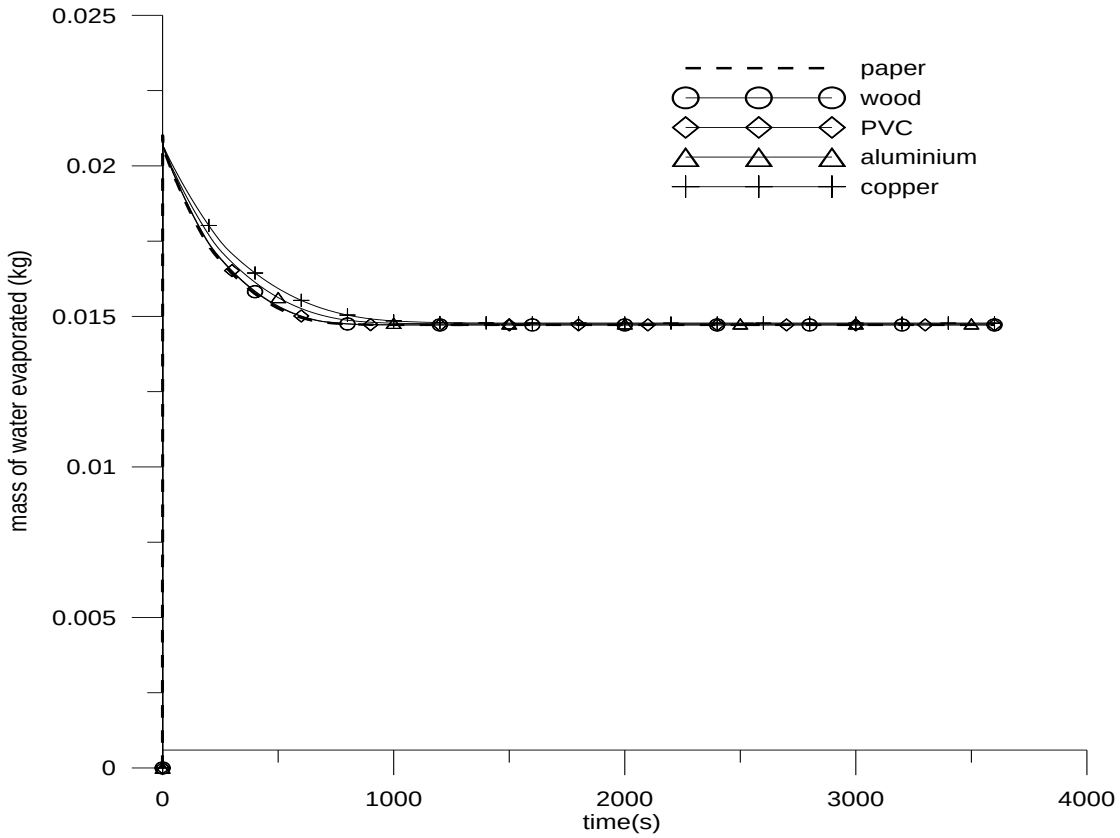

Figure 11: Mass of water evaporated for different packing materials at L = 0.1 kg/s and G = 2 kg/s.

In this part, we will study the effect of the pressure on the evaporation.

When the atmospheric pressure of the air is low, the air pushes harder on the surface of the water. The water molecules will then be easier to tear from the surface of the water to find themselves in the state of vapor. The temperature for which a pure liquid boils is named *'BOILING POINT'* (BP).

In this context we have varied the pressure within our co-current humidifier and it has been observed from curve 12 that the mass of water evaporated is greater when the pressure is lower.

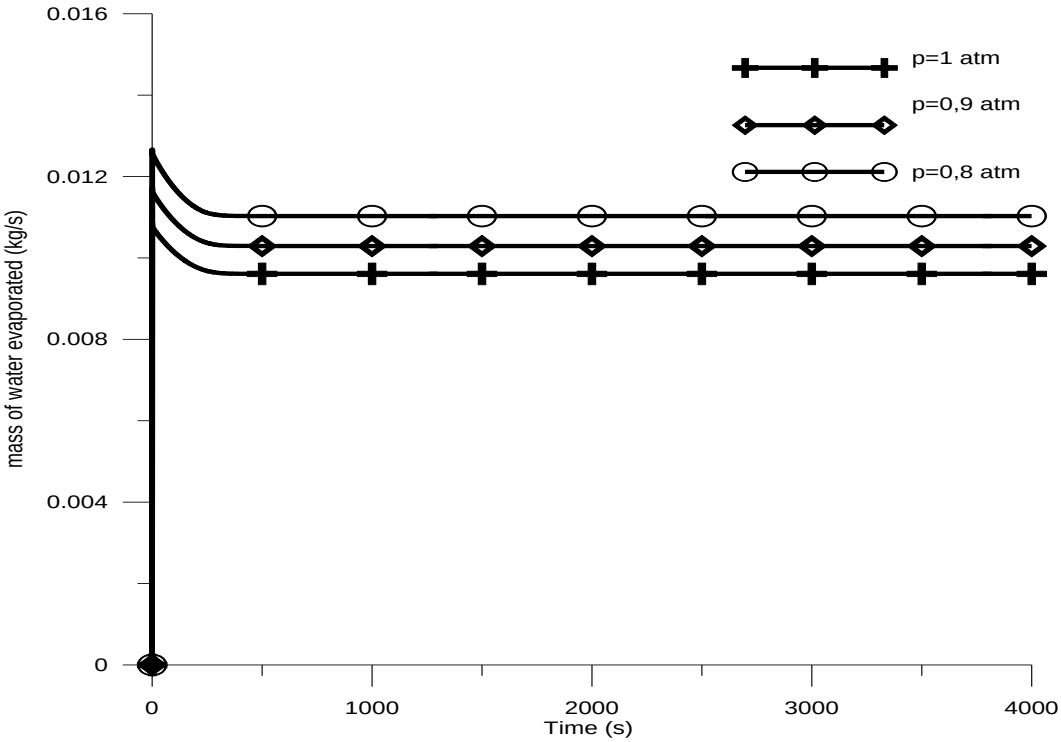

Figure 12: Mass of water evaporated for different pressure at L = 0.1 kg/s and G = 2 kg/s.

Then, for a fixed value of water and air flow rate, the air outlet temperature (figure 13) is higher if the pressure is lower and the water outlet temperature (figure 14) decreases when the pressure decreases.

So we observe that if a liquid is heated on lower pressure, the boiling point will be decreased which will also reduce the amount of heat energy needed to boil the liquid.

Therefore, when the pressure is reduced, the evaporation is considerable with certainly a gain of energy which is remarkable in terms of the outlet temperature of water and air.

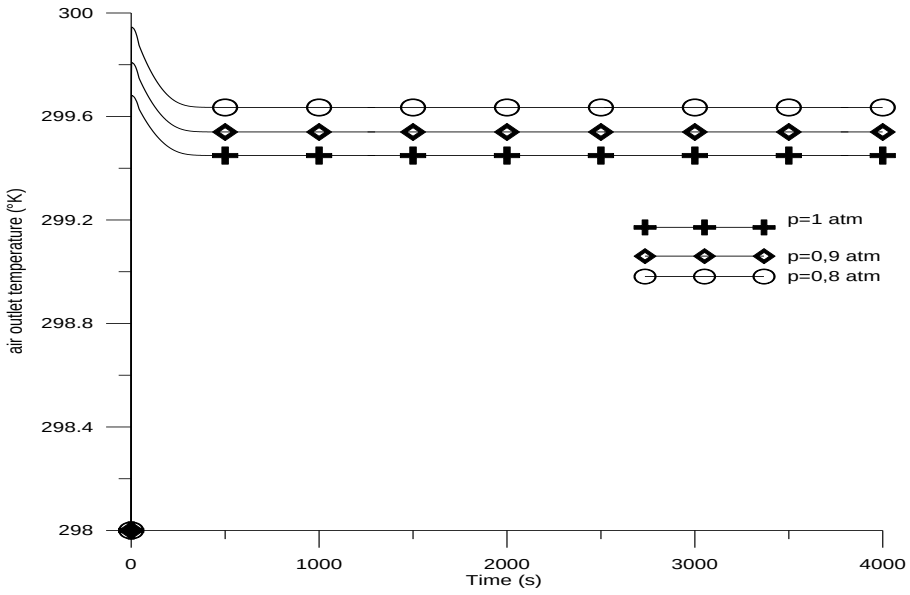

Figure 13: Air outlet temperature for different pressure at L = 0.1 kg/s and G = 2 kg/s.

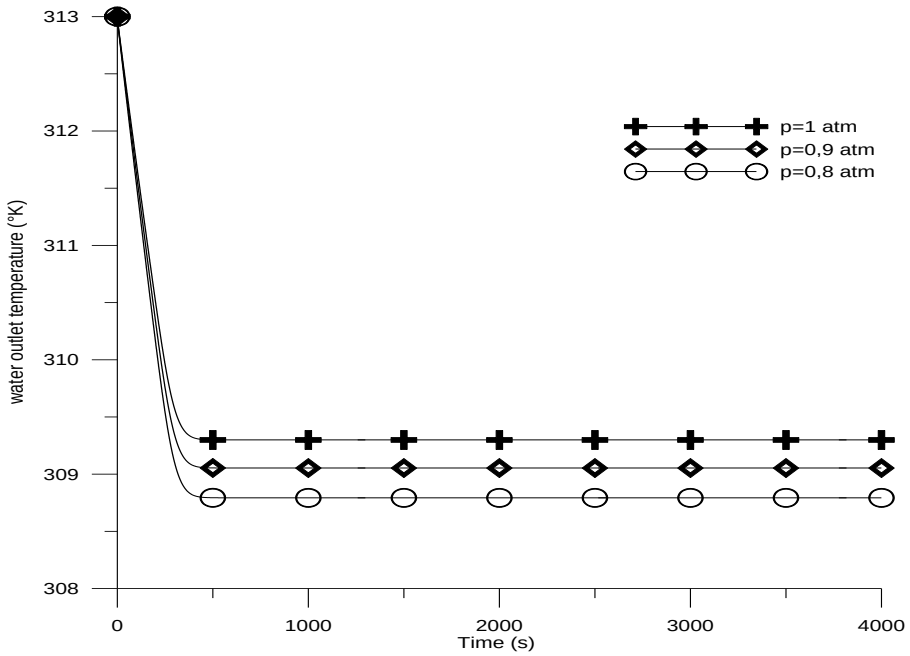

Figure 14: Water outlet temperature for different pressure at L = 0.1 kg/s and G = 2 kg/s.

4. Conclusion

Since co-current humidifiers are rarely published in the literature despite they are experimentally used, a co-current evaporator has been emphasized in this article by admitting it as a porous medium.

The mathematical model, which handles heat transfer and mass transfer, has been solved numerically using the finite volume method. The results were validated with experimental data from the literature. The comparison between the simplified and complete models explains the assumptions used.

The parametric study reveals that the humidification operation is optimal when considering a lower ratio L/G, an increasing in heat capacity and a high conductivity of the packaging material. Also a pressure vaporization within this humidifier shows that evaporation is done at lower temperatures at lower pressures than atmospheric pressure, from here horizons can be opened to systems multi-effect desalination MED

References

[1] M. Al-Sahali, H. Ettouney, Developments in thermal desalination processes design, energy, and costing aspects, Desalination 214 (2007) 227–240.

[2] A. Eslamimanesh, M.S. Hatamipour, Economical study of a small-scale direct contact humidification–dehumidification desalination plant, Desalination 250(2010)203–207.

[3] M. Mehrgoo, M. Amidpour, Constructal design of humidification–dehumidification desalination unit architecture, Desalination 271 (2011) 62–71.

[4] K. Bourouni, M.T. Chaibi, L. Tadrist, Water desalination by humidification and dehumidification of air: state of the art, Dealination, 137 (2001) 167-176.

[5] G. P. Narayan, M.H. Sharqawy, E.K.Summers, J.H. Lienhard, S.M. Zubair,M.A. Antar, The potential of solar-driven humidification-dehumidification desalination for small-scale decentralized water production, Renewable and Sustainable Energy Reviews, 14 (2010) 1187-1201.

[6] S. Hou, D. Zeng, S. Ye, H. Zhang, Exergy analysis of the solar multi-effect humidification-dehumidification desalination process, Desalination 203 (2007) 403-409.

[7] C. Yamali, I. Solmus, A solar desalination system using humidification-dehumidification process: experimental study and comparison with the theoretical results, Desalination, 220 (2008) 538-551.

[8] R.H. Xiong, S.C. Wang, L.X. Xie, Z. Wang, P.L. Li, experimental investigation of a baffled shell and tube desalination column using the humidification-dehumidification process, Desalination 180 (2005) 253-261.

[9] M. Ben Amara, I. Houcine, A. Guizani, M. Mâalej, experimental study of a multiple-effect humidification solar desalination technique, Desalination 170 (2004), 209-221.

[10] Y. J. Dai, H.F. Zhang, experimental investigation of a solar desalination unit with humidification and dehumidification, Desalination 130 (2000) 169-175.

[11] E. Chafik, A new type of seawater desalination plants using solar energy, Desalination 156 (2003) 333-348.

[12] M. M. Farid, A.W. Al-Hajaj, solar desalination with humidification-dehumidification cycle, Desalination 106 (1996) 427-429.

[13] N. K. Nawayseh, M.M. Farid, S. Al-Hallaj, A.R. Tamimi, Solar desalination based on humidification process. Part I. Evaluating the heat and mass transfer coefficients, Energy Conv. Manage., 40 (1999) 1423-1439.

[14] A. Eslamimanesh, M.S. Hatamipour, Mathematical modeling of a direct contact humidification–dehumidification desalination process, Desalination, 237 (2009) 296–304.

[15] M.M. Farid, S Parekh, J.R. Selman and S. Al-Hallaj, Solar desalination with a humidification–dehumidification cycle: mathematical modeling of the unit, Desalination, 151 (2002) 153–164.

[16] A.S. Nafey, H.E.S. Fath, S.O. El-Helaby and A.M. Soliman, Solar desalination using humidification-dehumidification processes, part I a numerical investigation. Energy Convers Manage, 45 (2004) 1243-1261.

[17] N. K. Nawayseh, M.M. Farid, A.A. Omar and A. Sabirin, Solar desalination based on humidification process-II. Computer simulation, Energy Convers Manage, 40 (1999) 1441-1461.

[18] H.E.S. Fath and A. Ghazy, Solar desalination using humidification–dehumidification technology, Desalination, 142 (2002) 119–133.

[19] S.A. El-Agouz, A new process of desalination by air passing through seawater based on humidification-dehumidification process, Energy 35 (2010) 5108-5114.

[20] Whitaker, S., Simultaneous Heat Mass and Momentum Transfer in Porous Media: A theory of drying, Academic press, 13(1977) 119-203

[21] S. Whitaker, A simple geometrical derivation of the spatial averaging theorem, Chem. Eng. Education 19 (1985) 18–21, 50–52.

[22] W.G. Gray, A derivation of the equations for multi-phase transport, Chem. Eng. Sci. 30 (1975) 229–233.

[23] ASHRAE Handbook of Fundamentals, American Society of Heating, Refrigerating, and Air-Conditioning Engineers, Inc, Atlanta, GA, 1997 Chapter 36.

[24] F. Gharagheizi, R. Hayati, S. Fatemi, Experimental study on the performance of mechanical cooling tower with two types of film packing, Energy Conversion and Management 48 (2007) 277–280

[25] P. Gao, L. Zhang, H. Zhang, Performance analysis of a new type desalination unit of heat pump with humidification and dehumidification, Desalination 220 (2008) 531-537.

[26] N. K. Nawayseh, M. M. Farid, A. A. Omar, S. M. Al-Hallaj, A. R. Tamimi, A simulation study to improve the performance of a solar humidificaion-dehumidification de salination unit constructed in Jordan, Desalination 109 (1997) 277-284.

[27] H. R. Goshayshi, J. F. Missenden, The investigation of cooling tower packing in various arrangements, App. Thermal Eng. 20 (2000) 69-80.

Tables

Figures